Visible light activation of room temperature NO_2 gas sensors based on ZnO, SnO_3 and In_2O_3 sensitized with CdSe quantum dots

Post-print version

Visible light activation of metal oxide semiconductors gas sensitivity

A.S. Chizhov, M.N. Rumyantseva, R.B. Vasiliev, D.G. Filatova, K.A. Drozdov, I.V. Krylov, A.V. Marchevsky, O.M. Karakulina, A.M. Abakumov, A.M. Gaskov

Publisher's version: A.S. Chizhov, et al., Visible light activation of room temperature NO_2 gas sensors based on ZnO, SnO_2 and In_2O_3 sensitized with CdSe quantum dots, Thin Solid Films http://dx.doi.org/10.1016/j.tsf.2016.09.029

Visible light activation of room temperature NO_2 gas sensors based on ZnO, SnO_2 and In_2O_3 sensitized with CdSe quantum dots

A.S. Chizhov[a], M.N. Rumyantseva[b*], R.B. Vasiliev[a,b], D.G. Filatova[b], K.A. Drozdov[c], I.V. Krylov[c], A.V. Marchevsky[a], O.M. Karakulina[d], A.M. Abakumov[b,d,e], A.M. Gaskov[b]

[a] Department of Materials Science, Moscow State University, Leninskie Gory 1-21, Moscow, 119991, Russia

[b] Chemistry Department, Moscow State University, Leninskie Gory 1-3, Moscow, 119991, Russia

[c] Physics Department, Moscow State University, Leninskie Gory 1-2, Moscow, 119991, Russia

[d] Electron Microscopy for Materials Research (EMAT), University of Antwerp, Groenenborgerlaan 171, B-2020 Antwerp, Belgium

[e] Skolkovo Institute of Science and Technology (Skoltech), Skolkovo Innovation Center, Moscow 143026, Russia

Abstract

This work reports the analysis of visible light activation of room temperature NO_2 gas sensitivity of metal oxide semiconductors (MOS): blank and CdSe quantum dots (QDs) sensitized nanocrystalline matrixes ZnO, SnO_2 and In_2O_3. Nanocrystalline metal oxides (MO_x) ZnO, SnO_2, In_2O_3 were synthesized by the precipitation method. Colloidal CdSe QDs were obtained by high temperature colloidal synthesis. Sensitization was effectuated by direct adsorption of CdSe QDs stabilized with oleic acid on MO_x surface. The role of illumination consists in generation of electrons, which can be transferred into MO_x conduction band, and holes that can recombine with the electrons previously trapped by the chemisorbed acceptor species and thus activate desorption of analyte molecules. Under green light illumination for blank SnO_2 and In_2O_3 matrixes the indirect consequential mechanism for the generation of holes is proposed. Another mechanism is realized in the presence of CdSe QDs. In this case the electron-hole pair is generated in the CdSe quantum dot. Sensor measurements demonstrated that synthesized materials can be used for NO_2 detection under visible (green) light illumination at room temperature without any thermal heating.

* Corresponding author. Tel: +7 495 939 54 71, Fax: +7 495 939 09 98. E-mail address: roum@inorg.chem.msu.ru

Keywords: room temperature semiconductor gas sensor; SnO_2; ZnO; In_2O_3; CdSe quantum dots; visible light activation; NO_2 detection

1. Introduction

The operating principle of semiconductor gas sensors is based on the high sensitivity of the electrical properties of semiconductors surface to the ambient atmosphere composition. However, the "solid – gas" reactions occur on the surface of metal oxide semiconductors (MOS) at rather high temperatures 100-500 ^oC. Such a temperature is necessary to increase the concentration of free charge carriers, for the activation of chemical reactions on the surface and for desorption of the reaction products. The need for heating substantially increases power consumption of semiconductor sensors that limits their use in stand-alone and portable devices, especially in communication systems like smartphones. Upon detection of oxidizing gases (NO_2, O_3) sensor signal generation occurs due to adsorption of analyte molecules on the metal oxide surface, which is accompanied by the localization of electrons on the adsorbed species lowering the electrical conductivity (for *n*-type semiconductors). At room temperature, this adsorption process is kinetically irreversible. The role of thermal heating upon NO_2 detection mainly consists in the activation of analyte molecules desorption and recovery of electrophysical properties of the sensitive material to initial state. In recent years, several reports on the use of photoactivation to increase MOS appeared. The vast majority of publications is devoted to study of MOS sensor properties under UV illumination [1 – 14]. The main obtained results were briefly summarized in Ref. [15]. Authors [11 – 13] demonstrated that illumination of a semiconductor metal oxide with UV-radiation is a good alternative to thermal heating to modulate the sensor signal value towards the oxidizing gases due to the photodesorption process.

A further reduction of power consumption is possible by using the radiation in the visible spectral range. However, bulk metal oxide semiconductors are transparent in this region of the spectrum. So, there are only few articles reported the room temperature gas sensor properties of blank nanocrystalline WO_3 [16], SnO_2 and ZnO [17] under visible light illumination. To increase MOS sensitivity to the visible light it is necessary to modify them with the photosensitizers capable to absorb such radiation. The role of sensitizers is to shift the optical sensitivity range of semiconductor oxides to higher wavelengths. Upon absorption of light photons with the energy greater than the band gap of the sensitizer an excitation of electron and its transition from the valence band to the conduction band occur. Then if photosensitizer and semiconductor oxide are in contact, a transition of an electron to the MOS conduction band becomes possible.

From a chemical point of view, all currently used photosensitizers of wide-gap semiconductors can be divided into three types: dyes, supramolecular complexes, and semiconductor quantum dots (QDs) [18]. The major advantage of the last ones is the possibility to adjust absorption spectral positions, extinction coefficients, etc. by simply changing of QDs size [19]. Effective charge transfer between QDs and wide band oxide semiconductor can be achieved by matching the conduction band of metal oxide and $1S_e$ size-dependent level of QDs (Fig. 1, [20, 21]). These materials are being actively studied in connection with their use in solar cells, but in the field of room temperature visible light activated semiconductor gas sensors only ZnO/CdS sensor properties were considered [22 – 24].

Our previous work [15] reported the study of oxygen controlled photoconductivity and visible light activated room temperature NO_2 gas sensors properties of nanocrystalline ZnO thick films sensitized with colloidal CdSe QDs. It was demonstrated that under green light illumination the electron-hole pair is generated in the CdSe quantum dot. Then photoexcited electron transfers to the conduction band of the semiconductor matrix while interarction of photoexcited hole can recombine with the electrons trapped by the chemisorbed $NO_{2(ads)}^{-}$, which loses its charge, becomes physically adsorbed, weakly coupled, and can be desorbed into gas phase even at room temperature. Present article is devoted to the analysis of visible light activation of room temperature NO_2 gas sensitivity of metal oxide semiconductors: blank and CdSe QDs sensitized nanocrystalline matrixes ZnO, SnO_2 and In_2O_3.

2. Experimental

2.1. Materials synthesis.

Nanocrystalline metal oxides (MO_x) ZnO, SnO_2, In_2O_3 were synthesized by the precipitation method [25 – 27]. To obtain nanocrystalline zinc oxide [25] $Zn(CH_3COO)_2$ solution was slowly added to a stirred solution of NH_4HCO_3 at 60 ºC. After aging for 1 h at room temperature, the $Zn_x(OH)_{2y}(CO_3)_{x-y}\cdot nH_2O$ precipitate (white powder) was centrifuged, washed with deionized water to remove residual ions and dried at 50 ºC for 24 h. ZnO powder was prepared by annealing the hydroxycarbonate at 300 ^oC for 24 hours in air.

Nanocrystalline samples of In_2O_3 were synthesized from $In(NO_3)_3\cdot 4.5H_2O$ which was dissolved in deionized water in an ice bath and 25% aqueous ammonia was slowly added to the stirred solution to achieve a complete precipitation of indium(III) hydroxide [26]. The resulting gel was centrifuged, washed several times with deionized water and dried at 100 °C during 24 h. In_2O_3 powder was prepared by annealing $In(OH)_3$ at 300 ^oC for 24 hours in air.

Nanocrystalline SnO_2 was prepared by conventional hydrolysis of tin (IV) chloride [27]. $SnCl_4*5H_2O$ was dissolved in deionized water and 25% aqueous ammonia was slowly added to the stirred solution to a complete precipitation of α-stannic acid. The resulting gel was centrifuged, washed with deionized water up to complete disappearance of the chloride ions ($AgNO_3$ test), and dried at 80 ^oC during 24 hours. The product was crushed and annealed in air at 300 ^oC for 24 hours.

For photoconductivity and sensor measurements nanocrystalline metal oxide powders were mixed with a vehicle (α-terpineol in ethanol) and deposited in the form of thick films over functional substrates, provided with Pt contacts on the front side and a Pt-meander that acts both as heating element and temperature probe, on the back-side. Thick films were dried at 30 ^oC for 24 hours and sintered at 300 ^oC for 10 hours in air.

Colloidal CdSe quantum dots were synthesized by a procedure reported previously [28] using oleic acid as a stabilizer. A mixture of $Cd(CH_3COO)_2$, oleic acid and octadecene was heated at 170 °C for 60 minutes under argon flow to remove acetic acid and water traces. Then the solution was heated up to 230 ^oC and Se precursor (freshly prepared 1M solution of selenium in trioctylphospine) was injected quickly. CdSe quantum dots were grown for 35 seconds. Then the reaction was stopped by rapid cooling down to room temperature. Finally, CdSe nanocrystals were precipitated from the solution by adding acetone. Then they were washed with acetone and redispersed in hexane. Precipitation-redispersion procedure was repeated 2-3 times to remove unreacted precursors and the excess of stabilizer.

Nanocomposites QD@MO_x were obtained by the direct attachment of CdSe QDs to the metal oxide surface. Sensitization was effectuated on MO_x powders (for composition and microstructure characterization and optical absorption investigations) and on MO_x thick films deposited over functional substrates (for photoconductivity and sensor measurements). Weighed MO_x powder (0.05 g) was immersed into 5 ml of hexane sol of CdSe QDs ($4*10^{-4}$ M) for 24 hours, washed with hexane to remove unattached QDs and finally dried in air. The volume and concentration of the sol were adjusted so that the amount of CdSe nanocrystals was 10 times higher than adsorption capacity of weighed MO_x powder.

Metal oxide thick films were immersed into hexane solution of CdSe QDs ($2.4*10^{-4}$ M) for 24 hours, washed with hexane and dried in air.

2.2. Materials characterization

Phase composition was examined by X-ray powder diffraction (XRD) with the Rigaku diffractometer (wavelength λ = 1.54059 Å (Cu Kα1 radiation)). MO_x crystallite size (d_{XRD}) was

calculated from the broadening of the most intensive XRD peaks using Scherer equation. The specific surface area was measured by nitrogen adsorption with the Chemisorb 2750 instrument (Micromeritics). The microstructure of the QD@MO_x composites was characterized by energy dispersive X-ray spectroscopy combined with scanning transmission electron microscopy (EDX-STEM) and high angular annular dark field STEM (HAADF-STEM) imaging. The study was performed at a FEI Osiris microscope operated at 200 kV and equipped with a Super-X detector.

The shape and size of the CdSe QDs were investigated using the transmission electron microscopy (TEM) performed with a LEO Omega 912AB microscope. The absorption spectra of the QDs colloidal solutions and sensitized MO_x powders in the wavelength range of 300-800 nm were recorded using Varian Cary 50 and Perkin Elmer Lambda 35 spectrometers, respectively.

Chemical composition of sensitized MO_x powders was analyzed by inductively coupled plasma mass spectrometry (ICP-MS) on a quadrupole ICP mass spectrometer (Agilent 7500c; Agilent Technologies, Waldbronn, Germany) [29]. Analytical signals were measured and data were processed using the built-in ChemStation software (G1834B version). Measurements were performed for isotopes $^{66, 68}Zn$, ^{115}In, $^{118, 120}Sn$, $^{110, 111, 112}Cd$, $^{77, 82}Se$. The designations of the samples, composition and microstructure parameters are given in Table 1.

The matching of composition of QD@MO_x powders and thick films was confirmed by X-ray fluorescent analysis (XRF) performed on M1 Mistral spectrometer (Bruker) with the beam energy of 50 keV. The diameter of the analyzed area was 1.0 mm, the signal accumulation time – 2 min. The measurements were performed separately for QD@MO_x powders and thick films deposited over functional substrates. The compositions coincidence was verified by the ratio of concentrations [Se]/[M], at. %.

Spectral dependence of photoconductivity of the sensitized films was investigated in a cell shielded from the background light. To illuminate the samples with narrow spectral band of radiation a combination of white light output 100 W/cm^2 with a monochromator MDR-206 was used. Photoconductivity was registered using a Keithley 6517 electrometer as a change of the sample conductivity under illumination. The samples were illuminated for 20 s at a certain radiation wavelength with a 60 min interval before the next measurement at a successive wavelength with 5 nm increment. The photoconductivity was calculated as a conductance ratio

$$\frac{\Delta\sigma}{\sigma_0} = \frac{\sigma(\lambda) - \sigma_0}{\sigma_0}, \quad (1)$$

where $\sigma(\lambda)$ is film conductance under illumination with corresponding λ, σ_0 - film conductance in dark conditions.

All sensor measurements have been carried out by flow through technique under a controlled constant flux of 100 ml/min. The atmosphere composition was pre-assigned by means of electronic mass-flow controllers (Bronkhorst). DC measurements (U = 3 V) have been carried out to monitor the electrical conductance of the sample during exposure to and NO_2/air gas mixtures (0.2 – 1.6 ppm NO_2 in dry air) under periodic green light illumination. Miniature LED of 20 mW/cm^2 power at the wavelength of excitonic transition of CdSe QDs λ_{max} = 535 nm was used as an illumination source. The linear character of current-voltage characteristics for the used voltage range was confirmed in Ref. [30].

3. Results and discussion

According to the results of the XRD analysis, the synthesized metal oxides are single phase nanocrystalline SnO_2 (cassiterite), ZnO (wurtzite) and In_2O_3 (bixbyite) (Fig. 2). Average crystallite diameters of MO_x obtained with the Scherrer formula (Table 1) increase in the row SnO_2 < In_2O_3 < ZnO. TEM images (Fig. 3 (a - c)) and crystal size distributions (Fig. 3 (d - f)) also indicate gradually increasing of MOx nanocrystals size.

Fig. 4a shows a typical TEM image of synthesized CdSe QDs. The QDs are nearly spherical with the mean diameter of 2.8 nm and narrow size distribution. The QDs exhibit absorption in the visible spectral range, with a sharp low-energy excitonic transition at λ = 535 nm (Fig. 4b).

SEM and optical images of the SnO_2 layer deposited over functional substrate and sintered at 300 ^oC are presented in Fig. 5a and Fig. 5b, respectively. One can see that the coating is continuous and uniform over the entire substrate. The estimated average film thickness is about 1 μm. The film is formed by the agglomerated particles and has a porous structure.

All MO_x samples after immersing in the colloidal solution of CdSe QDs acquired slightly orange coloration (Fig. 5c). Comparison of [Se]/[M] concentrations ratio obtained by X-ray fluorescent analysis for QD@MO_x powders and thick leads to the conclusion that the concentration of CdSe QDs in MO_x matrixes in form of powders and films is the same within accuracy of analysis (Table 1).

The presence of CdSe QDs in QD@SnO_2 and QD@ZnO powders was proved by HAADF-STEM imaging and EDX mapping in our previous studies [15, 28]. HAADF-STEM imaging and EDX analysis confirm attachment of the QDs to In_2O_3 grains (Fig. 6a). However, QDs distribution over metal oxide crystals is not uniform and there is a tendency for QDs to segregate (Fig. 6b).

The average density of CdSe QDs on MO_x surface (n_{QD}, QDs number per unit area of MO_x matrix, m^{-2}) was calculated from ICP-MS data as

$$n_{QD} = \frac{6 \cdot 10^{19} \cdot x \cdot M_{CdSe}}{\pi \cdot M_{MOx} \cdot \rho_{CdSe} \cdot d_{CdSe}^3 \cdot S_{surfMOx}}, \quad (2)$$

where $x = \frac{[Se]}{[M]}$ at.%; M_{MOx} – MO_x molar mass, g/mole; $S_{surfMOx}$ – MO_x specific surface area, m^2/g; M_{CdSe} – CdSe molar mass, 191 g/mole; d_{CdSe} – mean QDs diameter, 2.8 nm; ρ_{CdSe} – CdSe density, 5.81 g/cm^3.

This parameter decreases in the series QD@In_2O_3 > QD@ZnO >> QD@SnO_2 and for SnO_2 matrix the surface concentration of QDs is two orders of magnitude less than for ZnO and In_2O_3 based nanocomposites (Table 1). Such a difference cannot be explained only by the change of the specific surface area, which for SnO_2 is three times larger than for the other oxides. Apparently an additional effect of oxide surface wetting with non-polar solvent (hexane) is manifested. Since SnO_2 is more hydrophilic than the other oxides under consideration [31, 32], its surface is wetted worse with a non-polar solvent, which makes difficult the adsorption of quantum dots.

Spectral dependences of photoconductivity were tested to confirm contribution of QDs to photoconductivity as shown in Fig. 7. Photoconductivity and absorption spectra of nanocomposites demonstrate clear correlations. The maxima of photoresponse curve for nanocomposites matches well the maxima in corresponding absorption spectra. The onset of the absorption edge in the spectra of nanocomposites coincides with the appearance of the electrical photoresponse. The photoconductivity of pure ZnO and SnO_2 samples without QDs sensitization was negligibly small. For nanocrystalline SnO_2, obtained from aqueous media by the method used in this work, the measurements of photoconductivity at room temperature are difficult, since the current decreases continuously over time down to the values limited by sensitivity of the measurement device. This is due to significant contribution of the proton conductivity to the total value of the electrical conductivity of such samples [33, 34]. For that reason nanocomposites based on SnO_2 annealed at 700 °C were used for measurements. The photoconductivity of In_2O_3 sample is nonzero at photon energies lower than the optical band gap [26]. Photoresponse has been registered since the photon energy reaches 2.25 eV ($\lambda < 550$ nm). So, this sample is photosensitive to the green light. For all QD@MO_x samples the important photoconductivity increase is observed for the photon energy greater than 2.06 eV ($\lambda < 600$ nm)

indicating that the contribution of electrons excited in CdSe QDs to the photoconductivity can be decisive.

Our recent investigations [35] of the effect of CdSe QDs on the electrical properties of nanocrystalline In_2O_3 by impedance spectroscopy demonstrated that the addition of QDs substantially influences the resistance of interfaces between In_2O_3 crystals. However, the behavior of the frequency dependence of the samples conductivity is defined only by the nanocrystalline structure of semiconductor matrix. So, the addition of CdSe QDs does not modify the charge-carrier transport mechanism and induces only quantitative changes in the resistance due to charge (electron) transfer or through the energy transfer from CdSe QDs to the MO_x matrix with the excitation of electrons from local levels in the band gap of MO_x [36].

It was previously observed [15, 26] that when the light is turned on, the conductivity increases rather quickly but when the light is turned off, the conductivity recovers very slowly and full recovery can achieve several hours. So for gas sensor applications it is convenient to use the periodic illumination mode. The sensing properties of nanocomposites have been determined at room temperature by exposure to NO_2 with different concentration in dry air (Fig. 8). The LED (λ_{max} = 535 nm) in the sensor chamber was operated in a periodic mode and regularly switched on and off every 2 min. The resistance of sensing layer decreases during LED illumination and increases after switching off the LED. To discuss the obtained results it is necessary to compare the samples resistance $R(\lambda)_t$ after illumination (2 minutes) and $R(dark)_t$ after the following dark period (2 minutes). With the growing NO_2 concentration, both the $R(\lambda)_t$ and $R(dark)_t$ resistance values increase. The dynamic equilibrium between the processes

$$NO_{2(gas)} + e^- \leftrightarrow NO^-_{2(ads)} \text{ and} \quad (3)$$

$$NO^-_{2(ads)} + h^+ \leftrightarrow NO_{2(gas)} \quad (4)$$

determines the steady values of dark resistance $R(dark)_t$ and resistance under illumination $R(\lambda)_t$.

The amplitude of effective photoresponse $R(dark)_t/R(\lambda)_t$ at given NO_2 concentration is nearly constant. From these data the sensor signal was calculated as the ratio

$$S_{dark} = \frac{R(dark)_t}{R_0(dark)_t} \quad (5)$$

of dark resistances in pure air $R_0(dark)_t$ and at given NO_2 concentration $R(dark)_t$.

Blank In_2O_3 (Fig. 8a) and SnO_2 (Fig. 8b) demonstrate important and reproducible change of $R(\lambda)_t$ and $R(dark)_t$ depending on NO_2 concentration. The energy of light used in this work is about 2.3 eV, smaller than the SnO_2 and In_2O_3 band gap energy. However it has previously been reported that even light with energy lower than the band gap can induce photodesorption of

acceptor species due to the presence of sub-band surface states [37]. In this case the consequential mechanism for the generation of holes is realized: the photoholes are generated by photoinduced electron transition from ionized impurity levels to the conduction band, followed by thermal transitions of electrons from the valence band to empty acceptor levels. This mechanism is an indirect one and it depends both on the concentration of acceptor and temperature. It should be much weaker than the band gap mechanism and the corresponding threshold energy is E_g - E_a, where E_a is the ionization energy of the acceptor [38]. So, the photoexcited hole can recombine with the electrons trapped by the chemisorbed $NO_{2(ads)}^-$.

Another possibility for desorption of acceptor species is discussed in [16, 24, 39]. It consists in a direct absorption of the incident photon by a surface acceptor. The adsorption energy of the NO_2 on a metal oxide surface depends on the oxide crystallographic plane, presence of surface defects, mainly oxygen vacancies, and configuration of adsorbed species. The estimated values of NO_2 adsorption energy on SnO_2 surface varies, for example, from 0.48 to 1.37 eV for adsorption on SnO_2 nanoribbons [40], and from 0.85 eV (SnO_2 (110) surface) to 2.75 eV for adsorption on Al_2O_3 supported SnO_2 clusters [41]. In the case of NO_2 adsorption on ZnO nanotube the energy of 0.30 – 0.98 eV was found [42]. For NO_2 – ZnO interaction the type of crystallographic plane plays a crucial role. The NO_2 adsorption energy is 0.02 – 0.31 eV, 0.45 – 1.10 eV and 0.58 – 0.94 for ZnO $(2\bar{1}\bar{1}0)$, $(10\bar{1}0)$, and $(11\bar{2}0)$ plane, respectively [43, 44]. For NO_2 adsorption on In_2O_3 surface no information was found in the literature. In general we can conclude that green light photons (E = 2.3 eV) have enough energy to force NO_2 desorption. Probably the photodesorption of NO_2 occurs via two mentioned mechanisms in parallel but to determine the predominant one it is necessary to obtain some experimental proofs.

The effect of green light illumination on NO_2 photodesorption is not observed for blank ZnO samples studied in this work. The resistance of blank ZnO slightly increases when 0.2 ppm NO_2 appears in air and then does not change with the increase of NO_2 concentration (Fig. 8c). Effective photoresponse and sensor signal of ZnO is low and nearly constant for all NO_2 concentrations. This may be caused by high sample resistance (> 10^9 Ohm) in NO_2 containing atmosphere, which does not allow to make measurements reliably.

Among blank matrixes the maximum sensor signal is observed for nanocrystalline SnO_2 (Fig. 8) that correlates to its smallest particle size and largest surface area. The same tendency was previously observed for NO_2 sensor signal obtained under constant blue light illumination for SnO_2 and ZnO with specific surface area varied from 5 to 110 m^2/g [17] and under UV light for In_2O_3 samples with specific surface area of 10 – 100 m^2/g [45]. We can suppose that the

sample with the highest surface-to-volume ratio contains the largest number of defects which participate in the interaction with NO_2 molecules and the number of surface sites available for NO_2 adsorption is the main factor determining the resistance change in the presence of given concentration of acceptor gas.

Immobilization of CdSe QDs on ZnO surface leads to a decrease in samples resistance and to the appearance of reproducible change of $R(\lambda)_t$ and $R(dark)_t$ with NO_2 concentration (Fig. 8c). The photodesorption of NO_2 in this case may be due to interaction with the holes photogenerated in CdSe QDs (reaction (4)).

For SnO_2 matrix immobilization of CdSe QDs on its surface results in the decrease of sensor signal (Fig. 9). Therefore, the photodesorption of NO_2 due to interaction with the holes photogenerated in CdSe QDs becomes non effective. One possible reason of this effect may be the inactivation of photogenerated holes because of their interaction with hydrated species, which present on SnO_2 surface in a large amount [46].

In the case of In_2O_3 based nanocomposites introduction of QDs results in a decrease in resistance as for ZnO-based samples (Fig. 9). This indicates the transfer of an electron from the CdSe QD to the conduction band of In_2O_3. Among all the considered nanocomposites combination In_2O_3/CdSe has the maximum band offset between In_2O_3 and CdSe QDs (Fig. 1), which determines the electron injection rate [47]. That results in an increase in the amount of electrons transferred into matrix under illumination and in the augmentation in the concentration of electrons that can be captured by acceptor NO_2 molecule from In_2O_3 conduction band. In its turn this facilitates the reaction (1) and leads to an increase in the sensor signal. Moreover, for QD@In_2O_3 nanocomposites the both mechanisms of holes generation: due to the presence of sub-band surface states in In_2O_3 and from CdSe QDs – can be realized. This facilitates the reaction (4) and provides high effective photoresponse, which for practical use can be an alternative method of sensor signal measurement [15].

Conclusions

Photoconductivity and visible light activated room temperature gas sensors properties of nanocrystalline ZnO, SnO_2 and In_2O_3 thick films sensitized with colloidal CdSe QDs have been investigated. Sensor measurements were effectuated during exposure to 0.2 – 1.6 ppm NO_2 in dry air under periodic green light illumination using miniature LED as an illumination source. The role of illumination consists in generation of electrons, which can be transferred into MO_x conduction band, and holes that can recombine with the electrons previously trapped by the chemisorbed acceptor species and thus activate desorption of analyte molecules. Under green

light illumination for blank SnO_2 and In_2O_3 matrixes the indirect consequential mechanism for the generation of holes is realized: the photoholes are generated by photoinduced electron transition from ionized impurity levels to the conduction band, followed by thermal transitions of electrons from the valence band to empty acceptor levels. Another possible mechanism consists in a direct absorption of the incident photon by a surface acceptor resulting in NO_2 desorption. For blank matrixes the maximum sensor signal is observed for nanocrystalline SnO_2, which correlates to its highest surface-to-volume ratio providing the maximal number of surface sites available for NO_2 adsorption. A different mechanism is realized in the presence of CdSe QDs. In this case the electron-hole pair is generated in the CdSe quantum dot. Then photoexcited electron transfers to the conduction band of the semiconductor matrix while photoexcited hole can recombine with the electrons trapped by the chemisorbed $NO_{2(ads)}^{-}$. The most effective sensitization was achieved for In_2O_3 due to the maximum band offset between In_2O_3 and CdSe QDs. Moreover, only for QD@In_2O_3 nanocomposites the both mechanisms of holes generation can be realized. This provides high effective photoresponse, which for practical use can be an alternative method of sensor signal measurement. The obtained results indicate that nanocrystalline semiconductor oxides can be used for NO_2 detection under visible light illumination at room temperature without any thermal heating.

Acknowledgment

The work was financially supported by Russian Foundation of Basic Research grant No. 15-03-03026.

References

[1] J. Saura, Gas-sensing properties of SnO_2 pyrolytic films subjected to UV radiation, Sens. Actuat. B 17 (1994) 211–214.

[2] M. Law, H. Kind, B. Messer, F. Kim, P. Yang, Photochemical sensing of NO_2 with SnO_2 nanoribbon nanosensors at room temperature, Angew. Chem. Int. 41 (2002) 2405–2408.

[3] K. Anothainart, M. Burgmair, A. Karthigeyan, M. Zimmer, I. Eisele, Light enhanced NO_2 gas sensing with tin oxide at room temperature: conductance and work function measurements, Sens. Actuat. B 93 (2003) 580–584.

[4] T.-Y. Yang, H.-M. Lin, B.-Y. Wei, C.-Y. Wu, C.-K. Lin, UV enhancement of the gas sensing properties of nano-TiO_2, Rev. Adv. Mater. Sci. 4 (2003) 48–54.

[5] S. Mishra, C. Ghanshyam, N. Ram, R.P. Bajpai, R.K. Bedi, Detection mechanism of metal oxide gas sensor under UV radiation, Sens. Actuat. B 97 (2004) 387–390.

[6] E. Comini, L. Ottini, G. Faglia, G. Sberveglieri, SnO_2 RGTO UV activation for CO monitoring, IEEE Sens. J. 4 (2004) 17–20.

[7] C. Malagu, M.C. Carotta, E. Comini, G. Faglia, A. Giberti, V. Guidi, T.G.G. Maffeis, G. Martinelli, G. Sberveglieri, S.P. Wilks. Photo-Induced Unpinning of Fermi Level in WO_3, Sensors 5 (2005) 594-603.

[8] C.-H. Wan, D.-W. Hong, S.-D. Han, J. Gwak, K.C. Singh, Catalytic combustion type hydrogen gas sensor using TiO_2 and UV-LED, Sens. Actuat. B 125 (2007) 224–228.

[9] C. Ge, C. Xie, M. Hu, Y. Gui, Z. Bai, D. Zeng, Structural characteristics and UV-light enhanced gas sensitivity of La-doped ZnO nanoparticles, Mater. Sci. Eng. B 141 (2007) 43–48.

[10] B.P.J. de Lacy Costello, R.J. Ewen, N.M. Ratcliffe, M. Richards, Highly sensitive room temperature sensors based on the UV-LED activation of zinc oxide nanoparticles, Sens. Actuat. B 134 (2008) 945–952.

[11] J.D. Prades, R.J. Diaz, F. Hernandez-Ramirez, S. Barth, A. Cirera, A. Romano-Rodriguez, S. Mathur, J.R. Morante, Equivalence between thermal and room temperature UV light modulated responses of gas sensors based on individual SnO_2 nanowires. Sens. Actuat. B 140 (2009) 337-341.

[12] J.D. Prades, P. Jimenez-Diaz, M. Manzanares, F. Hernandez-Ramirez, A. Cirera, A. Romano-Rodriguez, S. Mathur, J.R. Morante, A model for the response towards oxidizing gases of photoactivated sensors based on individual SnO_2 nanowires, Phys. Chem. Chem. Phys. 11 (2009) 10881-10889.

[13] Ch.Y. Wang, R.W. Becker, T. Passow, W. Pletsche, K. Kohler, V. Cimalla, O. Ambacher, Photon-stimulated sensor based on indium oxide nanoparticles I: Wide-concedntration-range ozone monitoring in air, Sens. Actuat. B 152 (2011) 235-240.

[14] R. Bajpai, A. Motayed, A.V. Davydov, V.P. Oleshko, G.S. Aluri, K.R. Bertness, M.V. Rao, M.E. Zaghoul, UV-assisted alcohol sensing using SnO2 functionalized GaN devices, Sens. Actuat. B 171-172 (2012) 499-507.

[15] A.S. Chizhov, M.N. Rumyantseva, R.B. Vasiliev, D.G. Filatova, K.A. Drozdov, I.V. Krylov, A.M. Abakumov, A.M. Gaskov, Visible light activated room temperature gas sensors based on nanocrystalline ZnO sensitized with CdSe quantum dots. Sens. Actuators B 205 (2014) 305 – 312.

[16] C. Zhang, A. Boudiba, P. De Marco, R. Snyders, M.-G. Olivier, M. Debliquy, Room temperature responses of visible-light illuminated WO_3 sensors to NO_2 in sub-ppm range, Sens. Actuators B 181 (2013) 395–401

[17] E.V. Lukovskaya, O.A. Fedorova, Yu.A. Glazova, Yu.V. Fedorov, A.V. Anisimov, E.V. Podolko, M.N. Rumyantseva, A.M. Gaskov, F. Fages, Effect of light irradiation on the gas sensor characteristics of the SnO_2 and ZnO modified by tetrathiafulvalene derivative, Org. Photonics Photovolt. 3 (2015) 54 – 63

[18] A. Hagfeldt, G. Boschloo, L. Sun, L. Kloo, H. Pettersson, Dye-Sensitized Solar Cells, Chem. Rev. 110 (2010)6595–6663.

[19] P.V. Kamat, Quantum Dot Solar Cells. Semiconductor Nanocrystals as Light Harvesters, J. Phys. Chem. C 112 (2008) 18737-18753.

[20] D.S. Ginley, H. Hosono, D.C. Paine (Eds.) Handbook on trasparent conductors. Springer, 2011.

[21] S. Adachi. Properties of Group-IV, III-V and II-VI Semiconductors. Willey, 2005.

[22] J. Zhai, D. Wang, L. Peng, Y. Lin, X. Li, T. Xie, Visible-light-induced photoelectric gas sensing to formaldehyde based on CdS nanoparticles/ZnO heterostructures, Sens. Actuators B 147 (2010) 234-240.

[23] M.W.G. Hoffmann, A.E. Gad, J.D. Prades, F. Hernandez-Ramirez, R. Fiz, H. Shen, S. Mathur, Solar diode sensor: Sensing mechanism and applications, Nano Energy 2 (2010) 514-522.

[24] X. Geng, C. Zhang, M. Debliquy, Cadmium sulfide activated zinc oxide coatings deposited by liquid plasma spray for room temperature nitrogen dioxide detection under visible light illumination, Ceram. Int. 42 (2016) 4845 – 4852.

[25] N. Vorobyeva, M. Rumyantseva, D. Filatova, E. Konstantinova, D. Grishina, A. Abakumov, S. Turner, A. Gaskov, Nanocrystalline ZnO(Ga): Paramagnetic centers, surface acidity and gas sensor properties, Sens. Actuators B 182 (2013) 555 – 564.

[26] E.A. Forsh, A.M. Abakumov, V.B. Zaytsev, E.A. Konstantinova, P.A. Forsh, M.N. Rumyantseva, A.M. Gaskov, P.K. Kashkarov, Optical and photoelectrical properties of nanocrystalline indium oxide with small grains. Thin Solid Films 595 (2015) 25–31.

[27] M.N. Rumyantseva, A.M. Gaskov, N. Rosman, T. Pagnier, J.R. Morante, Raman surface vibration modes in nanocrystalline SnO_2 prepared by wet chemical methods: correlations with the gas sensors performances. Chem. Mater. 17 (2005) 893-901.

[28] R. Vasiliev, A. Babynina, O. Maslova, M. Rumyantseva, L. Ryabova, A. Dobrovolsky, K. Drozdov, D. Khokhlov, A. Abakumov, A. Gaskov, Photoconductivity of nanocrystalline SnO_2 sensitized with colloidal CdSe quantum dots, J. Mater. Chem. C 1 (2013) 1005–1010.

[29] D.G. Filatova, V.V. Es'kina, A.S. Chizhov, M.N. Rumyantseva, P.A. Shaposhnik, V.B. Baranovskaya, Yu.A. Karpov, Determination of selenium and cadmium in nanocomposites based on zinc and indium oxides by methods of high resolution continuous source electrothermal atomic absorption spectrometry and inductively coupled plasma mass spectrometry, J. Anal. Chem. 71 (2016) 496 – 499.

[30] R.B. Vasiliev, M.N. Rumyantseva, L.I. Ryabova, A.M. Gaskov, Conductivity of ultradispersed SnO_2 ceramic in strong electric fields, Semiconductors, 43 (2009) 156 – 157.

[31] M. Miyauchi, A. Nakajima, T. Watanabe, K. Hashimoto, Photocatalysis and Photoinduced Hydrophilicity of Various Metal Oxide Thin Films, Chem. Mater. 14 (2002) 2812-2816

[32] V. Rico, C. López, A. Borrás, J.P. Espinós, A.R. González-Elipe, Effect of visible light on the water contact angles on illuminated oxide semiconductors other than TiO_2, Solar Energy Mater. Solar Cells 90 (2006) 2944–2949

[33] R.B. Vasiliev, M.N. Rumyantseva, S.G. Dorofeev, Yu.M. Potashnikova, L.I. Ryabova, A.M. Gaskov, Crystallite size effect on the conductivity of the ultradisperse ceramics of SnO_2 and In_2O_3, Mendeleev Commun. 14 (2004) 167-169.

[34] R.B. Vasiliev, S.G. Dorofeev, M.N. Rumyantseva, L.I. Ryabova, A.M. Gaskov. Impedance spectroscopy of the ultradisperse SnO_2 ceramic with variable grain size. Semiconductors 40 (2006) 104 – 107.

[35] A.S. Il'in, N.P. Fantina, M.N. Martyshov, P.A. Forsh, A.S. Chizhov, M.N. Rumyantseva, A.M. Gaskov, P.K. Kashkarov, Effect of Cadmium-Selenide Quantum

Dots on the Conductivity and Photoconductivity of Nanocrystalline Indium Oxide, Semiconductors 50 (2016) 607–611.

[36] I.A. Akimov, Yu.A. Cherkasov, M.I. Cherkashin. Sensibilized Photoeffect. Nauka, Moscow, 1980. [in Russian].

[37] F. Messias, B. Vega, L. Scalvi, M. Li, C. Santilli, S. Pulcinelli, Electron scattering and effects of sources of light on photoconductivity of SnO_2 coatings prepared by sol‑gel, J. Non-Cryst. Solids 247 (1999) 171 – 175.

[38] L. Kornblit, A. Ignatiev, Photodesorption threshold energies in semiconductors, Surf. Sci. Lett. 136 (1984) L57 – L66.

[39] A. Giberti, C. Malagù, V. Guidi, WO_3 sensing properties enhanced by UV illumination: An evidence of surface effect, Sens. Actuators B 165 (2012) 56 – 61

[40] A. Maiti, J.A. Rodriguez, M. Law, P. Kung, J.R. McKinney,P. Yang, SnO_2 nanoribbons as NO_2 sensors: Insights from first principles calculations, Nano Lett. 3 (2003) 1025 – 1028

[41] Z. Liu, J. Li, S.I. Woo, H. Hu, Density functional theory studies of NO and NO_2 adsorption on Al_2O_3 supported SnO_2 cluster, Catal. Lett. 143 (2013) 912 – 918

[42] W. An, X. Wu, X.C. Zeng, Adsorption of O_2, H_2, CO, NH_3, and NO_2 on ZnO nanotube: A density functional theory study, J. Phys. Chem. C 112 (2008) 5747 – 5755.

[43] M. Breedon, M.J.S. Spencer, I. Yarovsky, Adsorption of NO and NO_2 on the ZnO $(2\bar{1}\bar{1}0)$ surface: A DFT study, Surf. Sci. 603 (2009) 3389 – 3399.

[44] J.D. Prades, A. Cirera, J.R. Morante, Ab initio calculations of NO_2 and SO_2 chemisorption onto non-polar ZnO surfaces, Sens. Actuators B 142 (2009) 179 – 184

[45] A. Ilin, M. Martyshov, E. Forsh, P. Forsh, M. Rumyantseva, A. Abakumov, A. Gaskov, P. Kashkarov, UV effect on NO_2 sensing properties of nanocrystalline In_2O_3, Sens. Actuators B 231 (2016) 491 – 496

[46] A.V. Marikutsa, M.N. Rumyantseva, E.A. Konstantinova, T.B. Shatalova, A.M. Gaskov, Active sites on nanocrystalline tin dioxide surface: Effect of palladium and ruthenium oxides clusters, J. Phys. Chem. C 118 (2014) 21541 – 21549.

[47] I. Robel, M. Kuno, P.V. Kamat. Size-Dependent Electron Injection from Excited CdSe Quantum Dots into TiO_2 Nanoparticles, J. Am. Chem. Soc. 129 (2007) 4136-4667.

Figure captions:

Fig. 1. Scheme of the mutual arrangement of the energy levels for bulk In_2O_3, SnO_2, ZnO and CdSe: conduction band E_C, valence band E_V, band gap E_g, electron affinity χ_c, level of photoexcited electron $1S_e$, level of photoexcited hole $1S_h$.

Fig. 2. XRD patterns of SnO_2, In_2O_3 and ZnO samples.

Fig. 3. TEM images and crystal size distributions for SnO_2 (a, d), In_2O_3 (b, e) and ZnO (c, f) samples.

Fig. 4. TEM image (a) and optical absorption spectrum (b) of 2.8 nm CdSe QDs stabilized with oleic acid.

Fig. 5. Images of thick films deposited over functional substrate and sintered at 300 ^oC: (a) SnO_2 layer, SEM image; (b) SnO_2 layer, optical image; (c) ZnO and QD@ZnO layers, optical image.

Fig. 6. HAADF-STEM image and EDX-STEM maps demonstrating QD at the surface of the In_2O_3 particles: (a) magnification 630k; (b) magnification 225k. The maps are presented in counts.

Fig. 7. Absorption spectra and spectral dependences of photoconductivity of QD@MOx nanocomposites.

Fig. 8. Room temperature electrical resistance of (a) In_2O_3- , (b) SnO_2- and (c) ZnO-based samples under periodic green light illumination (λ_{max} = 535 nm) depending on NO_2 content in the gas phase. (1) – data for blank matrixes, (2) – data for QD@MO_x nanocomposites.

Fig. 9. Sensor signal $S_{dark} = R(dark)_t / R_0(dark)_t$ of In_2O_3- ,SnO_2- and ZnO-based samples under periodic green light illumination (λ_{max} = 535 nm) depending on NO_2 content in the gas phase. Open symbols – data for blank matrixes, filed symbols – data for QD@MO_x nanocomposites.

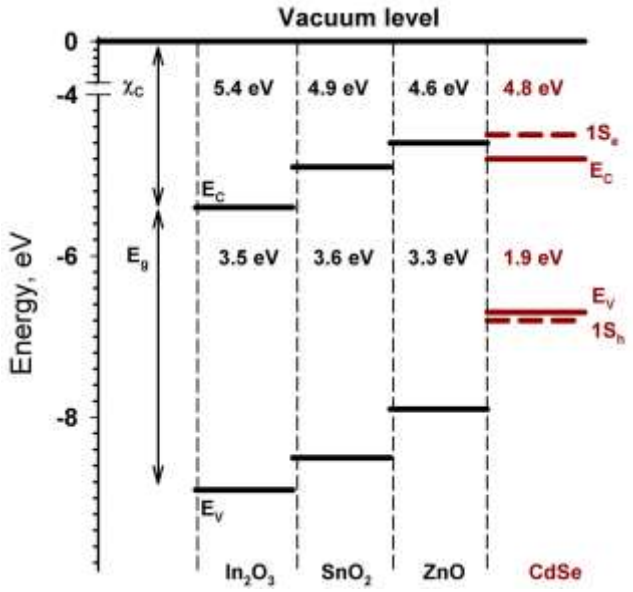
Vacuum level
0
-4
-6
-8
Energy, eV
χc
Eg
5.4 eV
4.9 eV
4.6 eV
4.8 eV
3.5 eV
3.6 eV
3.3 eV
1.9 eV
1Se
EC
EC
EV
EV
1Sh
In2O3
SnO2
ZnO
CdSe

Fig. 1

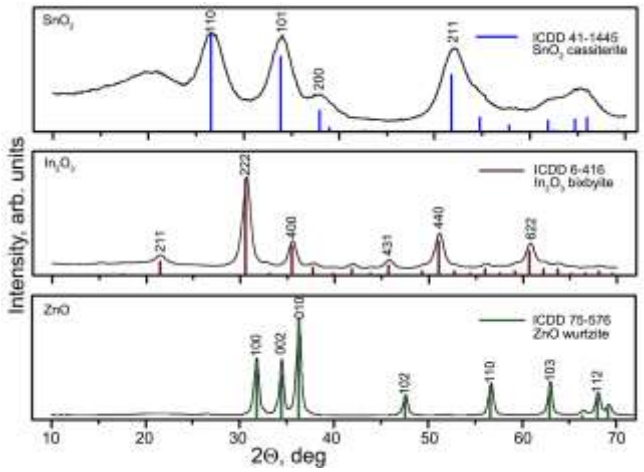
SnO2
ICDD 41-1445
SnO2 cassiterite
110
101
200
211
In2O3
ICDD 6-416
In2O3 bixbyite
222
211
400
431
440
622
ZnO
ICDD 75-576
ZnO wurtzite
100
002
010
102
110
103
112
Intensity, arb. units
10
20
30
40
50
60
70
2Θ, deg

Fig. 2

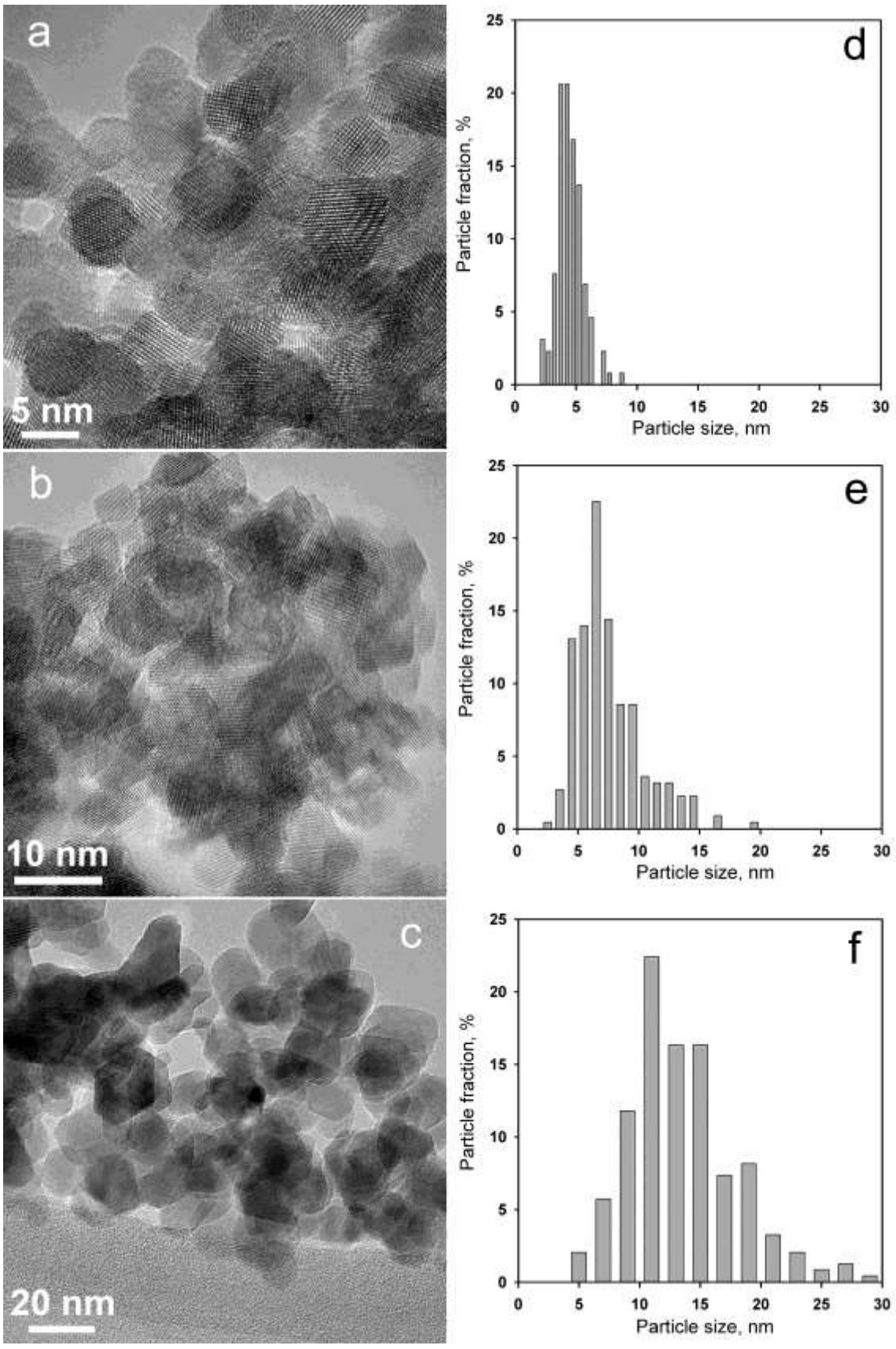
a
5 nm
b
10 nm
c
20 nm
d
e
f
Particle fraction, %
Particle size, nm
0
5
10
15
20
25
30
Fig. 3

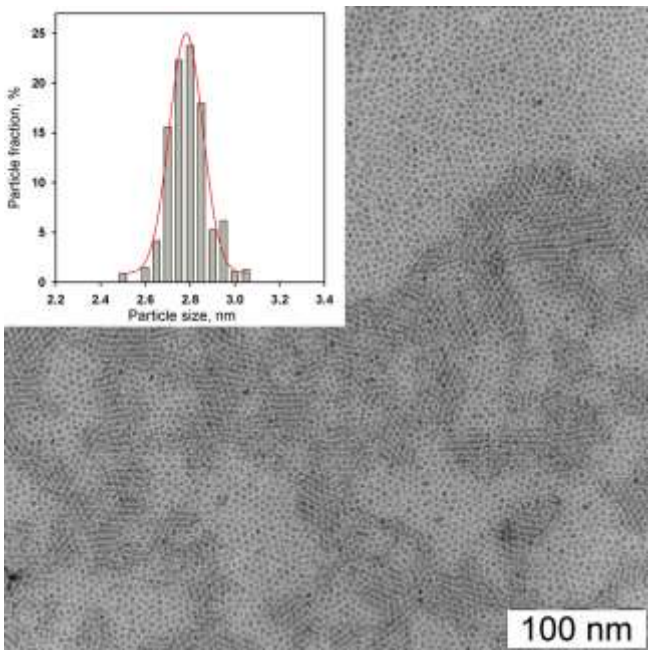
Particle fraction, %
Particle size, nm
100 nm

Fig. 4a

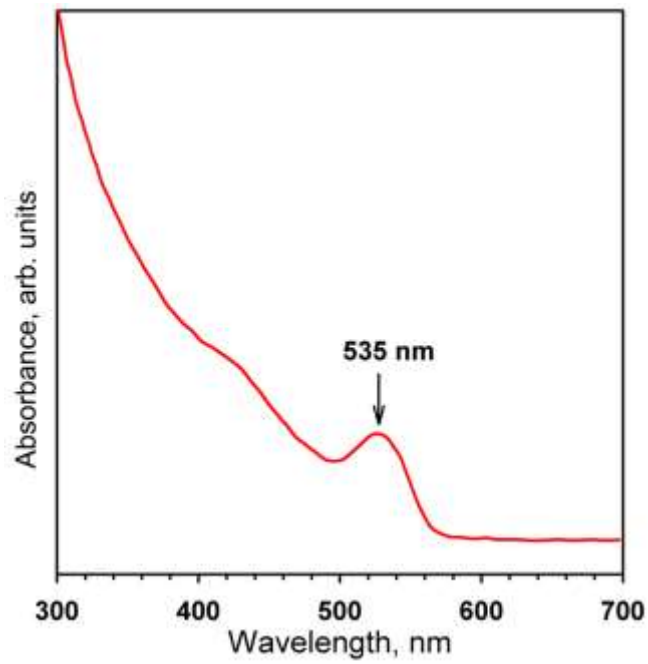
Absorbance, arb. units
535 nm
Wavelength, nm

Fig. 4b

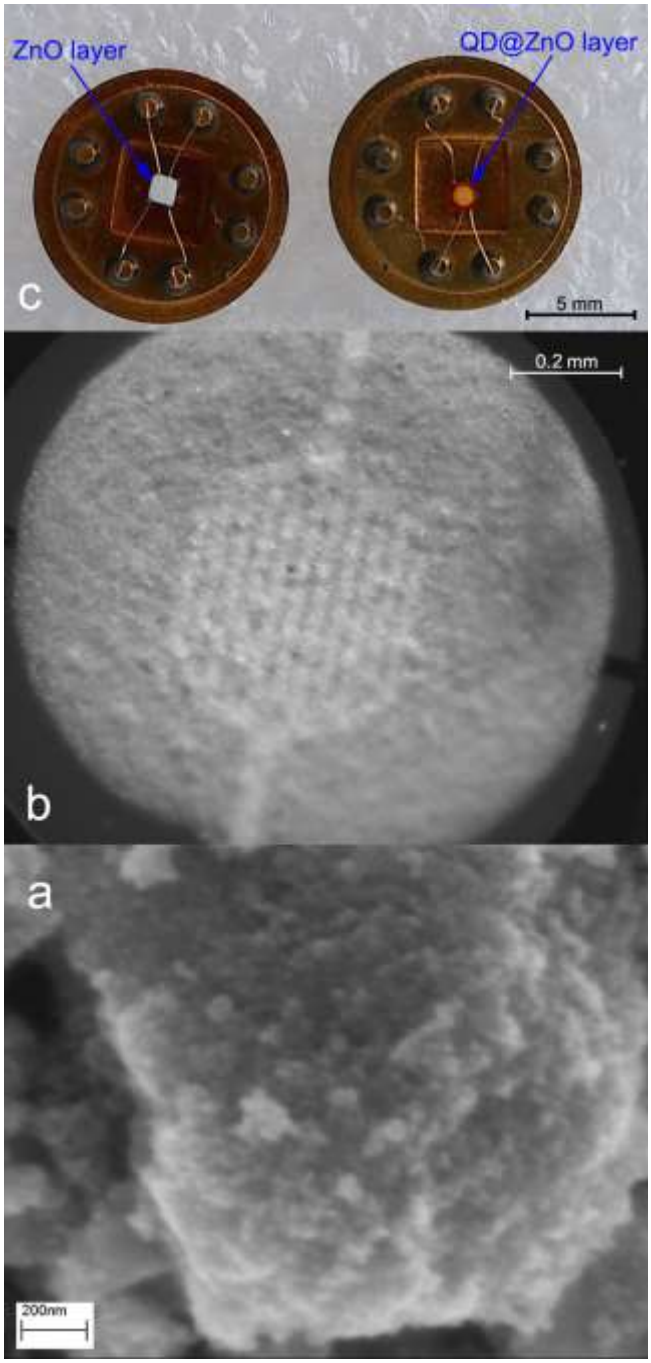

Fig. 5

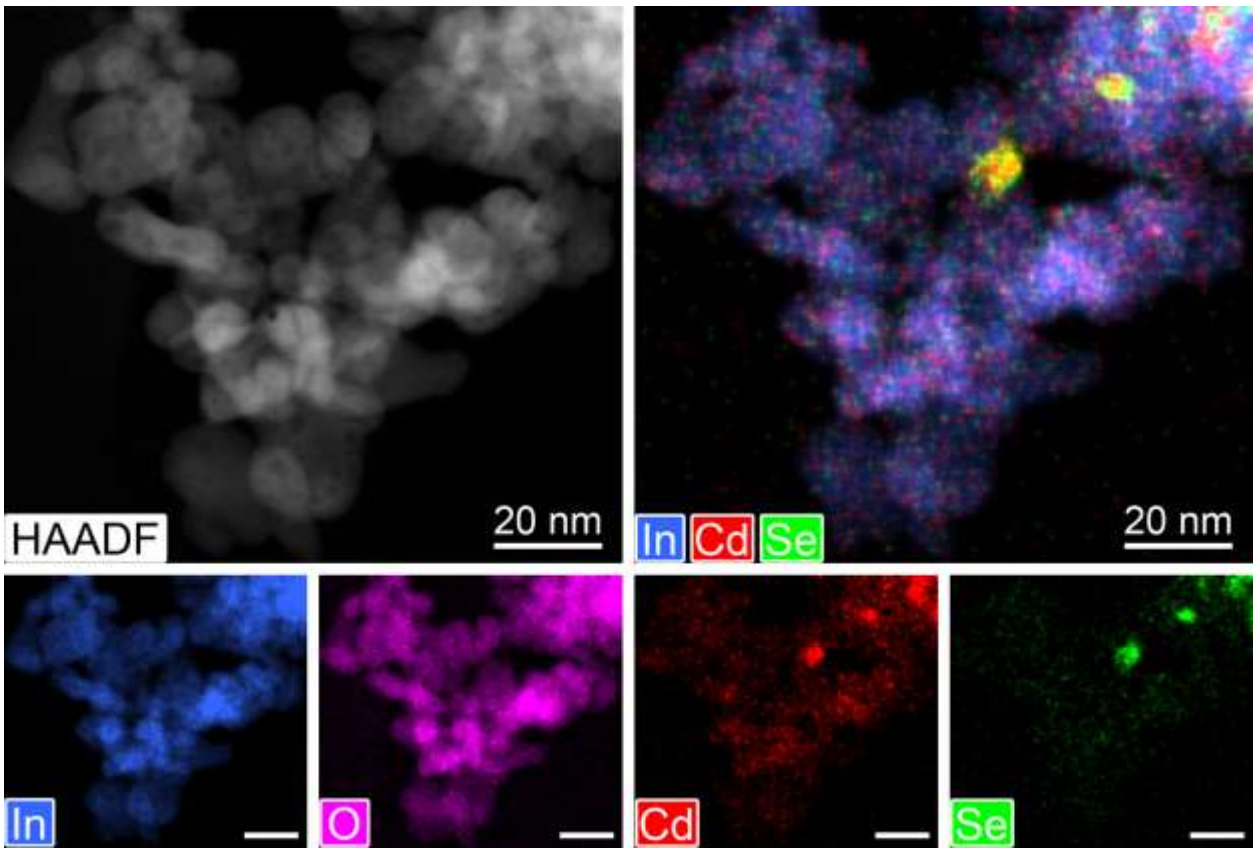
HAADF
20 nm
In Cd Se
20 nm
In
O
Cd
Se
Fig. 6a

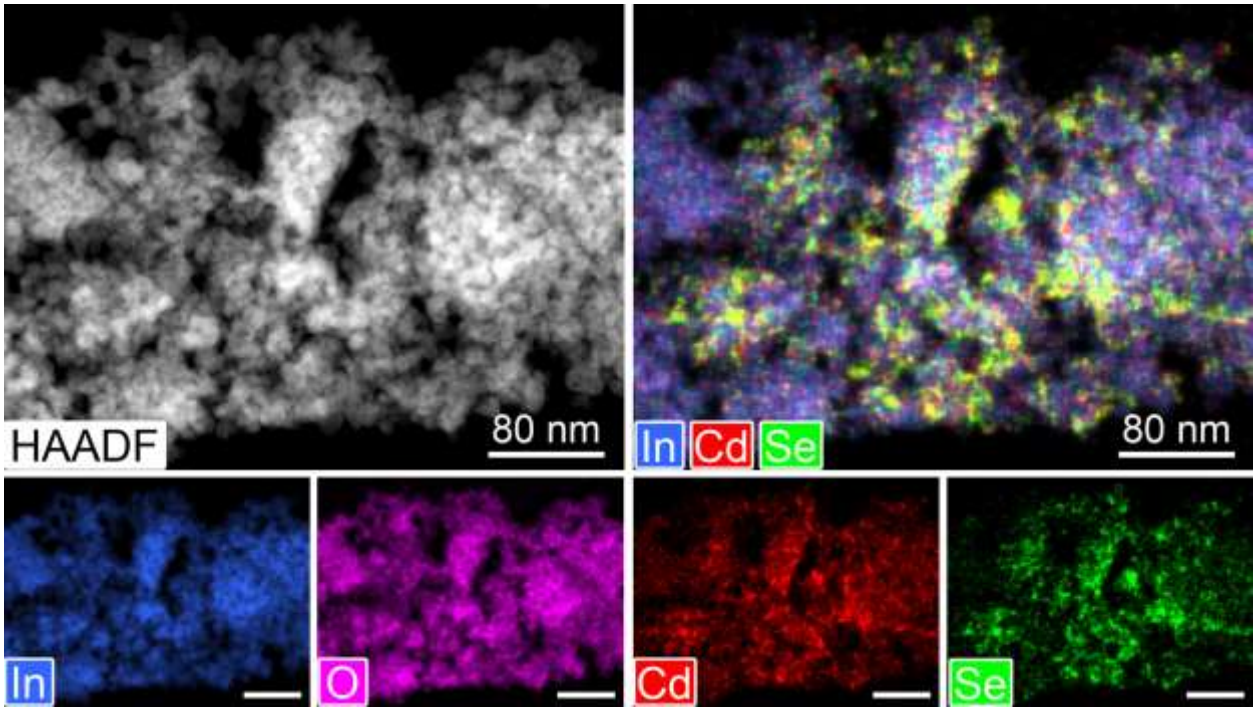
HAADF
80 nm
In Cd Se
80 nm
In
O
Cd
Se
Fig. 6b

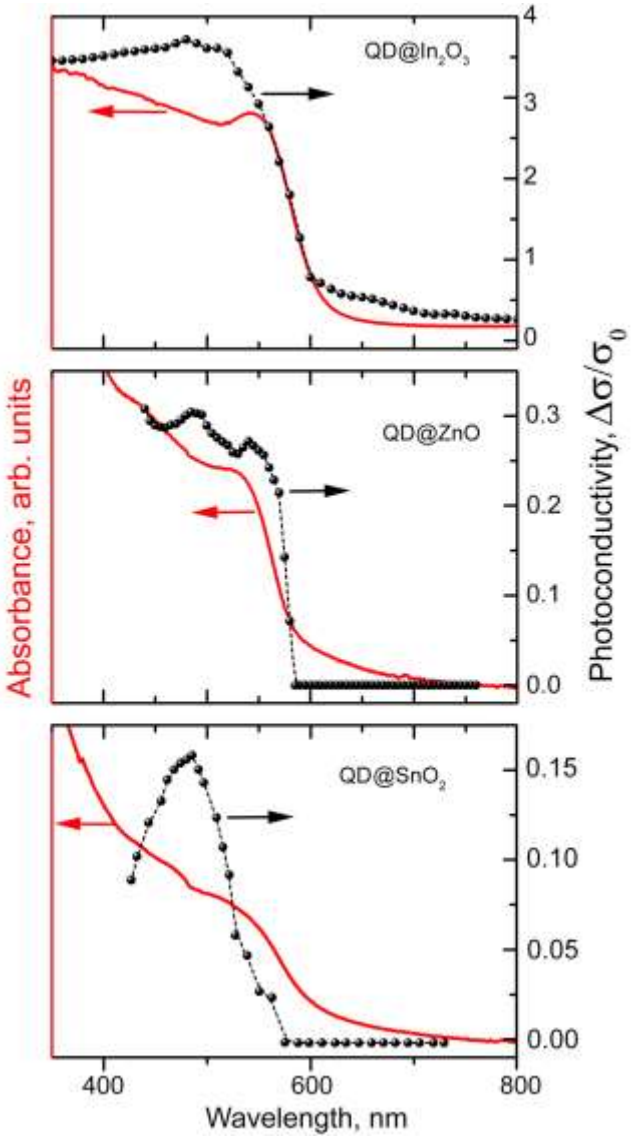
QD@In2O3
QD@ZnO
QD@SnO2
Absorbance, arb. units
Photoconductivity, Δσ/σ0
Wavelength, nm
400
600
800
0
1
2
3
4
0.0
0.1
0.2
0.3
0.00
0.05
0.10
0.15

Fig. 7

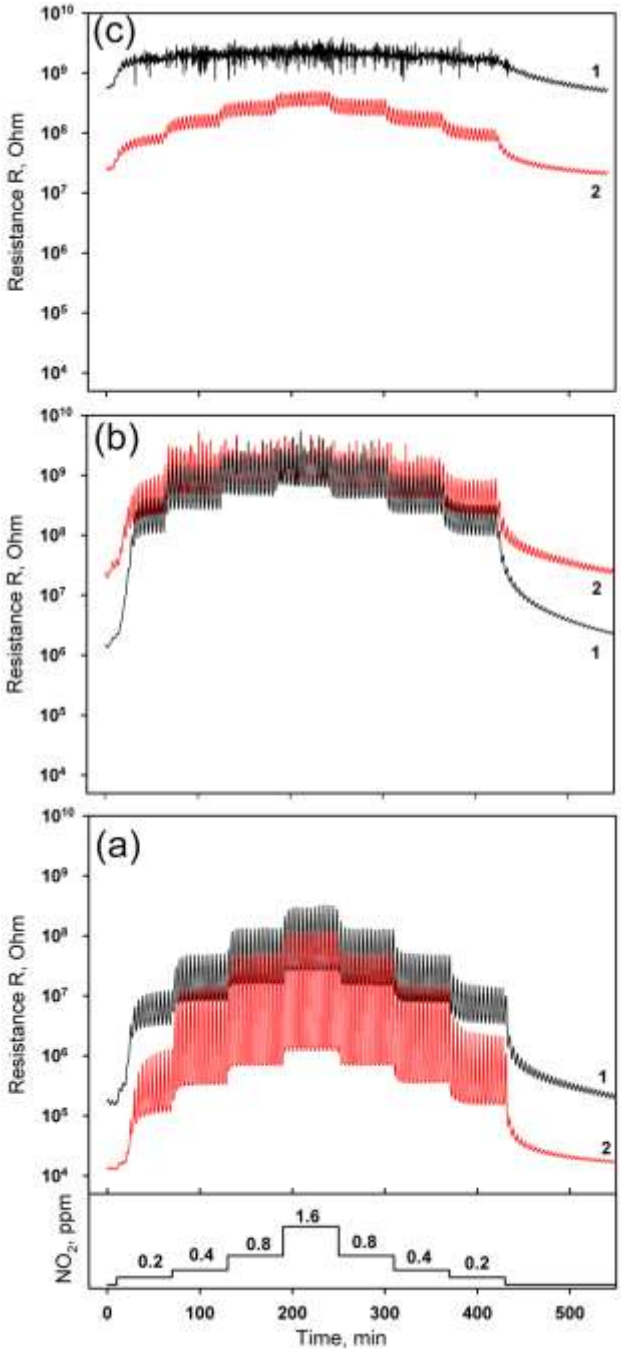
(c)
(b)
(a)
Resistance R, Ohm
1
2
NO2, ppm
0.2
0.4
0.8
1.6
0.8
0.4
0.2
0
100
200
300
400
500
Time, min

Fig. 8

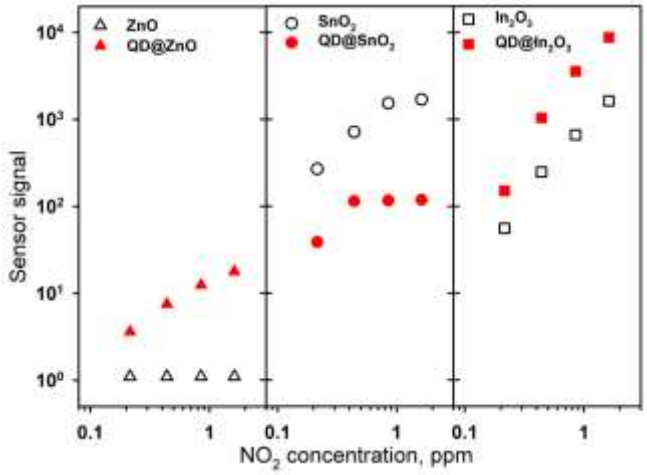
ZnO
QD@ZnO
SnO2
QD@SnO2
In2O3
QD@In2O3
Sensor signal
NO2 concentration, ppm

Fig. 9